Bourikas et al. Future Cities and Environment (2016) 2:7
DOI 10.1186/s40984-016-0020-4

Future Cities and Environment

TECHNICAL ARTICLE Open Access

Transforming typical hourly simulation weather data files to represent urban locations by using a 3D urban unit representation with micro-climate simulations

Leonidas Bourikas[1*], Patrick A. B. James[1], AbuBakr S. Bahaj[1], Mark F. Jentsch[2], Tianfeng Shen[3], David H. C. Chow[4] and Jo Darkwa[5]

Abstract

Urban and building energy simulation models are usually driven by typical meteorological year (TMY) weather data often in a TMY2 or EPW format. However, the locations where these historical datasets were collected (usually airports) generally do not represent the local, site specific micro-climates that cities develop. In this paper, a humid sub-tropical climate context has been considered. An idealised "urban unit model" of 250 m radius is being presented as a method of adapting commonly available weather data files to the local micro-climate. This idealised "urban unit model" is based on the main thermal and morphological characteristics of nine sites with residential/institutional (university) use in Hangzhou, China. The area of the urban unit was determined by the region of influence on the air temperature signal at the centre of the unit. Air temperature and relative humidity were monitored and the characteristics of the surroundings assessed (eg green-space, blue-space, built form). The "urban unit model" was then implemented into micro-climatic simulations using a Computational Fluid Dynamics – Surface Energy Balance analysis tool (ENVI-met, Version 4). The "urban unit model" approach used here in the simulations delivered results with performance evaluation indices comparable to previously published work (for air temperature; RMSE <1, index of agreement d > 0.9). The micro-climatic simulation results were then used to adapt the air temperature and relative humidity of the TMY file for Hangzhou to represent the local, site specific morphology under three different weather forcing cases, (ie cloudy/rainy weather (Group 1), clear sky, average weather conditions (Group 2) and clear sky, hot weather (Group 3)). Following model validation, two scenarios (domestic and non-domestic building use) were developed to assess building heating and cooling loads against the business as usual case of using typical meteorological year data files. The final "urban weather projections" obtained from the simulations with the "urban unit model" were used to compare the degree days amongst the reference TMY file, the TMY file with a bulk UHI offset and the TMY file adapted for the site-specific micro-climate (TMY-UWP). The comparison shows that Heating Degree Days (HDD) of the TMY file (1598 days) decreased by 6 % in the "TMY + UHI" case and 13 % in the "TMY-UWP" case showing that the local specific micro-climate is attributed with an additional 7 % (ie from 6 to 13 %) reduction in relation to the bulk UHI effect in the city. The Cooling

(Continued on next page)

* Correspondence: L.Bourikas@soton.ac.uk
[1]Energy & Climate Change Division, Sustainable Energy Research Group (SERG), Faculty of Engineering and the Environment, University of Southampton, Southampton SO17 1BJ, UK
Full list of author information is available at the end of the article

(Continued from previous page)
Degree Days (CDD) from the "TMY + UHI" file are 17 % more than the reference TMY (207 days) and the use of the "TMY-UWP" file results to an additional 14 % increase in comparison with the "TMY + UHI" file (ie from 17 to 31 %). This difference between the TMY-UWP and the TMY + UHI files is a reflection of the thermal characteristics of the specific urban morphology of the studied sites compared to the wider city. A dynamic thermal simulation tool (TRNSYS) was used to calculate the heating and cooling load demand change in a domestic and a non-domestic building scenario. The heating and cooling loads calculated with the adapted TMY-UWP file show that in both scenarios there is an increase by approximately 20 % of the cooling load and a 20 % decrease of the heating load. If typical COP values for a reversible air-conditioning system are 2.0 for heating and 3.5 for cooling then the total electricity consumption estimated with the use of the "urbanised" TMY-UWP file will be decreased by 11 % in comparison with the "business as usual" (ie reference TMY) case. Overall, it was found that the proposed method is appropriate for urban and building energy performance simulations in humid sub-tropical climate cities such as Hangzhou, addressing some of the shortfalls of current simulation weather data sets such as the TMY.

Keywords: Idealised urban unit model, Micro-climate simulations, Urban weather projections, Cities

Introduction

Engineering and urban design practise often relies on thermal simulation modelling in order to achieve regulatory compliance and support decision making on urban and building design, as well as sizing of building energy systems that directly effects energy consumption. Urban and building energy simulation models are usually driven with hourly weather datasets for a 'typical' year [1]. In humid sub-tropical climates where air-conditioning is the primary concern the year format is that of an "average year" (eg TMY2 or EPW). Common typical weather year formats have the form of a synthetic year which is compiled from multiple years to be representative of the climatic conditions for the site of interest [2].

Heating, Ventilation and Air Conditioning (HVAC) systems are often oversized in order to reduce design risk by ensuring that the system will cope with loads above the average year's design day estimations [3]. This affects the energy consumption of the building, potentially the thermal comfort of the users and the indoor air quality, whilst at the same time increasing the cost of operation and possibly maintenance for building services [4].

The main concern in the case of building energy systems' oversizing is the way that energy use is estimated, more specifically the heating, cooling, dehumidification and mechanical ventilation loads. At the moment, in many countries, weather data files with a typical meteorological year (TMY2 or EPW) format are used for building regulation compliance calculations [5]. However, compliance to the regulations does not necessarily ensure occupants' satisfaction or represent the real operational conditions of the building services. One important consideration for the use of the typical year weather time series in energy consumption predictions and simulations is the representativeness of the location where the source data have been collected. Many of these locations are, due to historical data availability, airports near large cities. However, locations within the city develop local, site specific micro-climates that will not always be represented by these datasets [6].

Over recent decades many cities have expanded rapidly through higher building densities, larger building heights and growth towards suburban and rural areas. This expansion results in changes to the balance of the urban energy budget [7] which consists of the radiation, sensible, latent and anthropogenic heat fluxes and the roughness caused by the built environment [7]. These features of the built environment's energy and mass equilibrium can cause atmospheric forcing which alters the local weather conditions [8] and contributes to the development of distinctive local micro-climates specific to a site's characteristics and morphology. The micro-climatic factor with the most noticeable variation regarding changes in the energy budget is the air temperature [9]. The urban air temperature (T) difference to the regional non-urban air temperature (eg airport sites) is defined as the urban heat island (UHI) and the magnitude of this difference is known as the urban heat island intensity (UHII) [10].

Field observations and experimental measurements have been used by various researchers in order to create algorithms for the adaptation of weather data to local specific morphologies [11–13]. In Hong Kong, urban heat island intensity observations were used in order to adapt a weather data file and use it in cooling load simulations [14]. In a field study, Wong et al. [15] pointed out that density, the ratio of building height to building footprint area and especially the green surface area (vegetation) can substantially influence the development of the micro-climate. Summertime temperature observations in London suggest additional correlations of UHI intensity with the distance from a thermal hotspot and wind direction [16].

More recently, a model was introduced for the estimation of the UHI intensity in urban centres and the

modification of weather data files in the UK [17]. This model is based on the statistical analysis of temperature data from UK based weather stations from the period 1961 to 2006. The urban thermal centres were defined by assigning thresholds to predefined urban fraction parameters for each UK grid cell and its surroundings [17]. The urban fraction limits were calibrated with visual inspection of the fit of calculated ranges for the urban fraction parameters to real UK cities [17]. Therefore, in order to apply this methodology in places other than the UK, this method should be repeated for similar or equivalent local land cover types and temperature data spatial resolution under the same baseline assumptions of urban fraction limits.

In a numerical weather prediction approach, the Urban Canyon model [18] estimates the heat fluxes and the air temperature distribution in an urban street canyon configuration. It introduces a zonal model that divides the air volume between the buildings into cells where the heat and mass balance can be estimated for each cell [18]. The results have been used to introduce the climatic severity index (CSI) that can assess the impact of the street canyon morphology on the heating and cooling demands of locally based buildings [18].

In a very interesting development, meso-scale weather forecasting and numerical weather prediction-CFD models were coupled in order to predict the micro-scale weather development in wind farms and urban environments [19, 20]. In these coupling schemes, the numerical weather prediction models were downscaled in order to provide the initial and boundary conditions for the micro-scale models [21]. Despite the benefits from coupling meso- to micro-scale models, the differences in the horizontal and vertical scales and the time resolution between these models pose a challenge to their widespread successful application. The grid size differences and subscale grid implications regarding the physical processes at play are often a threat to the analysis of the results and their correct physical interpretation [22]. In addition, numerical models are computationally demanding in terms of both power and time. Therefore, their use in micro-scale modelling is usually restricted to small domains and relatively simple geometries [23].

A more common approach is the coupling of numerical weather prediction models with analytical micro-scale models. The analytical urban canopy models estimate the energy balance development and momentum transfer in relation to the urban canopy's morphology and produce single area-averaged values in order to be used as forcing in the scale (typically meso-scale) that the weather prediction model resolves [24]. Ren et al. [25] have created a "morphed" TMY file for the city of Melbourne using a regional weather forecasting model coupled with an urban canopy parameterisation scheme for the prediction of monthly changes due to the UHI effect in air temperature, RH and wind speed [25]. The Town Energy Balance and an integrated building energy model have been coupled with other schemes (ie rural station, vertical diffusion and urban boundary layer model) and they have been used for the adaptation of rural air temperature and relative humidity hourly values to the urban heat island effect [26]. The so-called Urban Weather Generator requires a large number of initial parameters that vary from construction elements properties and characteristics (eg albedo and initial temperature) to the urban (eg façade to site ratio) and reference rural site morphology [27]. The land cover analysis for the creation of the simplified "urban unit model" can provide most of the required parameters for the initialisation of the Urban Weather Generator. The use of the 3D "urban unit model" in numerical simulation modelling was chosen instead as it can provide an approximation of the vertical development of air temperature and relative humidity in the roughness sublayer and it can capture the majority of the transient physical processes at street level.

The aim of this study is to provide a comprehensive methodology that allows for an integration of urban micro-climate conditions into standard weather datasets such as the TMY. In order to achieve this, this paper introduces an idealised "urban unit model" (on a 250 m radius) that represents the main thermal and morphological characteristics of urban sites at street level in the neighbourhood scale. This model, which was produced using statistical land cover and urban morphology analysis, can be used with simulations as a method of adapting commonly available weather data files to a local specific micro-climate. This methodology is used to adapt air temperature and relative humidity (RH) from the TMY file to the effects of local site specific morphology on urban weather development. The "urban weather projections" resulting from this adaptation were then used for comparing the degree days amongst the reference TMY file, the TMY file offset for a bulk hourly UHI intensity (local) and the TMY adapted for the urban weather projections (local + micro). Finally, the TMY file generated by this methodology was used for the dynamic thermal simulation of heating and cooling loads in a domestic and a non-domestic building scenario. The potential improvements in the estimation of building energy consumption were assessed against the business as usual case of applying typical meteorological year data files in places with a humid sub-tropical climate such as the case study city of Hangzhou in China.

Methodology

An important issue for the successful application of any existing micro-climatic model are the input data

prerequisites. Detailed information on the surface materials' properties, morphological and other modelling parameters is not however, always readily available. There is a need for models to estimate the weather conditions within urban areas as a function of time and urban morphology [28, 29]. The "urban unit model" introduced above has, therefore, been designed to be as general as possible in order to facilitate widespread use in building thermal and urban design simulations. Ideally, a visual evaluation (or an automated GIS platform) would be used to decide the urban class for the site of interest. This would be enough to enable offsetting of the reference (TMY or real time non-urban) hourly air temperature (T) and relative humidity (RH) for the selected urban class for different seasonal weather forcing.

A small size neighbourhood was selected as the scale of interest. An "urban unit" has been defined as an area forming disk (with a radius of 250 m) around the centre of a neighbourhood where a temperature and relative humidity sensor was located. Air temperature and relative humidity were monitored at 26 urban sites in Hangzhou (30°15'N 120°10'E) in Zhejiang Province, China [30, 31]. The sensors were installed on lampposts at a level 3 to 5 m above ground. They logged air temperature at 11-Bit (0.0625 °C) resolution and relative humidity at 12-Bit (0.04 %) resolution [32]. The manufacturer stated air temperature accuracy is +/-0.5 °C and the RH accuracy is +/- 5 % RH [32]. For calibration purposes, air temperature (°C) and RH (%) readings within 1 min intervals were compared to the readings of two separate thermocouples in an environmental chamber at -10, 0, 10 and 40 °C [33]. All sensors operated within the reported accuracy margin and fitted well to the thermocouple measurements [33].

According to Oke [34] air temperature and relative humidity observations in the surface layer (3x above average building height) can be expected to be representative of an area ranging from 100 m to several hundred meters in a direction upwind and around each sensor. It is to be expected that most of the sensors were collecting measurements in the roughness sub-layer and not in the surface layer [35] (Table 1). The location of the

Table 1 Siting of selected sensors in Hangzhou and representation of the size of the "urban unit" (Top Right)

Siting of the sensor (blue bullet point)

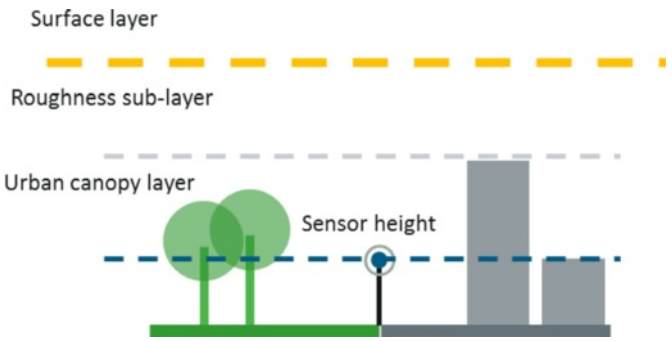

Circle of influence

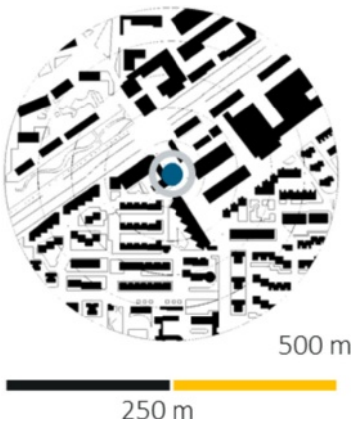

Sensor on a lamppost close to a tall building wall

Sensor on a lamppost next to a road

measurement sites was carefully selected to have as homogeneous characteristics as possible for a large city and the sensors were installed a reasonable distance away from sites of noticeable surface type change [30].

The urban unit's size, ie the radius of the disk around the "centre of a neighbourhood", has been determined by assessing the vegetation cover's influence on air temperature. For this, twelve urban sites were selected across the city centre of Hangzhou, North of the Qiantang River (Fig. 1).

Each sensor was considered to be the centre of concentric circles at radii of 10, 25, 50, 100, 150, 200, 300, 400 and 500 m. The footprint of the vegetated surface was estimated and apportioned to these annular areas. The analysis was carried out for 14 weeks of hourly data collected during summer 2013. The air temperature (Tair) in Fig. 2 is the average air temperature departure from the mean temperature of the 12 sensors in this group for this 14 week period. The vertical shaded reference line marks the 250 m radius from the centre (ie the sensor). The legend shows the mean summer air temperature departure from the group's mean and the goodness of fit of the non-linear regression line in parentheses.

It is to be expected that the influence of green-space is larger when closer to the sensor and that it diminishes if it is more towards to the outer annular areas. This is shown in Fig. 2. The strong influence of vegetated areas close to the sensor is evident from the first peak of a vegetated surface area in comparison to the general trend in the group of sensors. The locations of sensors 3 (dark green; -1.4 °C) and 10 (purple; -0.4 °C) have a lower than the group average air temperature and their vegetated surface area is large with an early peak within the first 100 m from the sensor (Fig. 2). Interestingly, sensor 12 (dark cyan; -1.0 °C) which also shows a negative temperature departure from the group mean has a small vegetated area approximately 150 m away from the sensor, comparable with those at locations with higher than the group average temperature. Its negative trend can, however, probably be explained with the steep rise in vegetated surface area at the annular area from 150 to 200 m, showing that the influence of vegetation remains strong at this distance (Fig. 2).

Further evidence comes from the comparison between sensor 1 (black, +0.5 °C) and sensors 2, 5 and 9 (pink, red, gold; +0.2 °C). The regression trend lines indicate that the location where sensor 1 resides is warmer than the locations of sensors 2, 5 and 9 despite the larger vegetated surface within a 0 to 100 m radial distance from the sensor. In the case of sensors 2, 5 and 9 the vegetated surface area peaks occur later at distances from 100 to 150 m showing the persistent impact of the green-space area. In addition, site 5 (red; +0.2 °C) has a similar vegetated surface area to site 1 (black; +0.5 °C) with the only difference being a delay of the peak, that is seen at distances 50 to 100 m farther out. Sensor 11 (dark blue, -0.2 °C) has a lower air temperature than the group average but the green-space percentage peak occurs after the 250 m radius border. However, in this case the low air temperature is mainly attributed to the site's proximity to a large wetland (ie Xixi). Based on these results a representative circular "urban unit" has been defined with a 250 m radius. It is expected that the total

Fig. 1 Location of the 12 sites for the urban unit size assessment (Left) and a typical fisheye image used for estimating the Sky View Factor in Hangzhou (Right). (Note: The Mantou Mountain, National Principle Weather station's location (reference, typical meteorological year file source) is marked as NP. The colour scheme of the bullet points in the map is consistent with Fig. 2

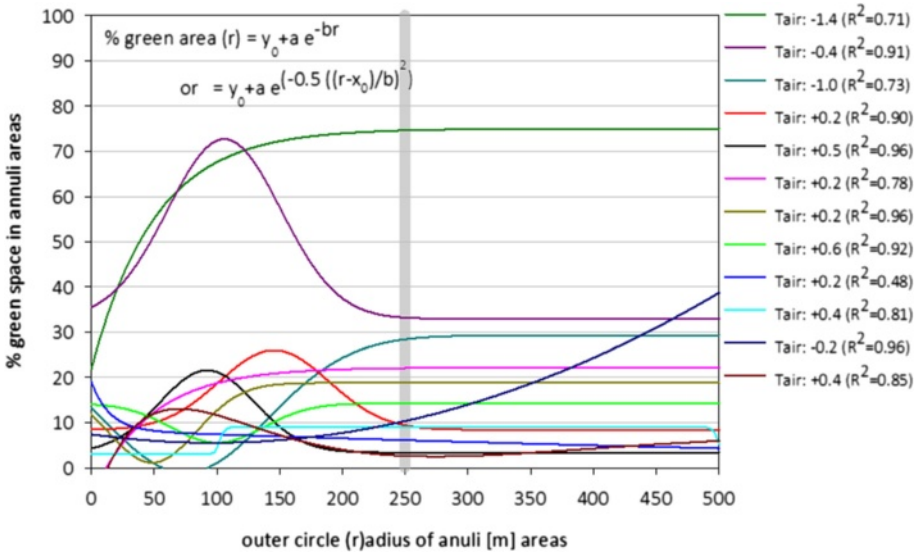

Fig. 2 Regression lines of the percentage vegetated area in each annular area on the distance from the centre (ie the sensor)

area of about 200,000 m^2 (250 m radius) surrounding the sensor will be the representative part of the source area for the air temperature and relative humidity signal. The size of the proposed urban unit also agrees with other authors' studies on the windward distance from a point of roughness or thermal change (~200–500 m) and the internal boundary layer extent in zones within local climate classification schemes (r ~ 200–500 m) [36].

Building on the urban unit as defined above, this study adopted a combination between a local urban classification scheme and the simulation of the local specific weather development for urban unit layouts in the case study region with a residential/institutional (university, college) use. Micro-climatic simulation modelling was used to assess the influence of the neighbourhoods' morphology on the local, street level air temperature. The main advantage of using such a surface classification scheme is that it provides generic input data for the simulation model [36] and that the simulation results can be attributed back to typical urban morphology characteristics.

There are three key parts to the methodology for generating the "urban weather projections" that result from the combined urban classification and simulation modelling (Fig. 3): (Step 1) The creation of the idealised "urban unit model" for the sites of interest (in this study 9 sites); (Step 2) The normalisation of the reference weather data with the local monthly UHI patterns for different weather forcings and (Step 3); The adaptation of the UHI adjusted hourly air temperature and RH data to account for the effect of the site specific generic morphology at street level at the neighbourhood scale.

These three components of the overall methodology are described in the following:

Step 1. A simplified model for urban micro-climatic simulations

The generation of the "urban unit model" is based on the following steps:

(1) The land cover analysis starts with the inspection and selection of an aerial image of the sensor's location in Google Earth [37]. The image with the best orthographic projection and quality is selected (ideally, a clear top plan view image). It is then processed with SketchUp [38], a computer aided design software, using the urban unit described above with the data logger at the centre of the 250 m circular area (Fig. 4).

(2) A selection of metadata (eg high resolution images taken on site) is used in combination with the aerial view to draw polygons for the vegetation (green colour), water (blue colour) and built-up (black colour) surfaces (Fig. 4). The residual is designated as other impermeable surface (white colour) and includes street and pavement surfaces. A set of morphological parameters is then calculated for each site including: the mean building height $\bar{H}$, the roughness length z_0, the height to width aspect ratio, the frontal area ratio λ_f, the building surface fraction F_r, the impervious surface fraction I_r and the pervious surface fraction P_r.

(3) Each urban site is classified according to the land cover analysis into a "Local Climate Zone" following an urban classification scheme developed by Stewart and Oke [36]. Each zone (ie thermally homogenous region of uniform surface characteristics) in the scheme exhibits a distinctive diurnal temperature

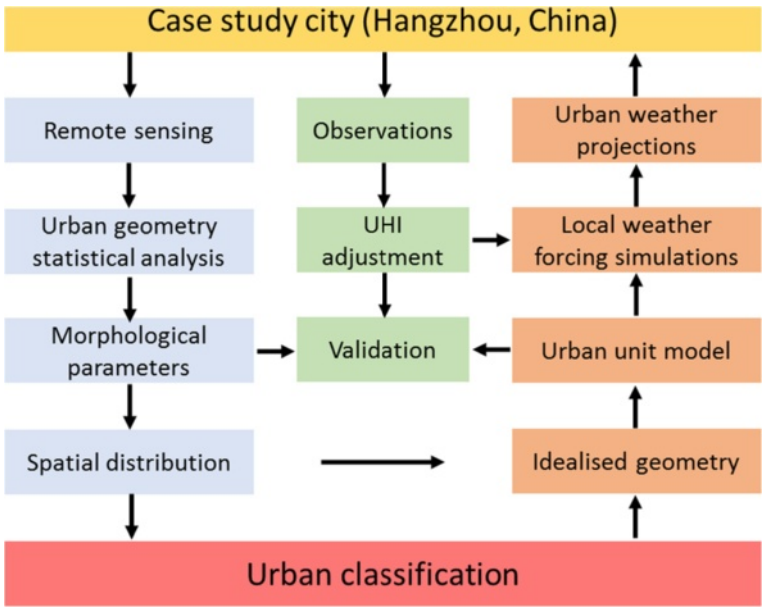

Fig. 3 Methodology for adapting TMY files to include the effect of the local site specific morphology in cities

development profile at sensor height (~1.5 to 3 m) at the local scale [36]. The resulting Local Climate Zones (LCZs) describe 17 generic environments consisting of 10 zones for built-up (eg open high-rise) and 7 for non-urban land cover types (eg scattered trees) [36]. Each zone is represented by a set of ten morphological parameters and a descriptive definition of the typical location and use of the urban sites classified into a zone. Nine urban sites out of a total of 26 investigated areas in Hangzhou were classified as "Local Climate Zone 5" (LCZ5) (Fig. 5) which denotes midrise buildings at a medium density arrangement [36]. This study focuses on these nine sites classified as "LCZ5".

(4) The urban morphology of these sites is further analysed for 5 annular areas. The annular rings' periphery has been defined at radii of 50, 100, 150, 200 and 250 m. Urban morphological parameters and descriptive statistics are then calculated for all the annular areas (ie 0–50 m (red), 50–100 m (orange), 100–150 m (blue), 150–200 m (green), 200–250 m (outer) as shown in Table 2, for an example of site 2 in Fig. 5).

(5) The generic, idealised "urban unit model" is constructed to have a similar planar area ratio and mean weighted (footprint) building height to the nine studied sites. The individual surface energy balances are represented in the model by the

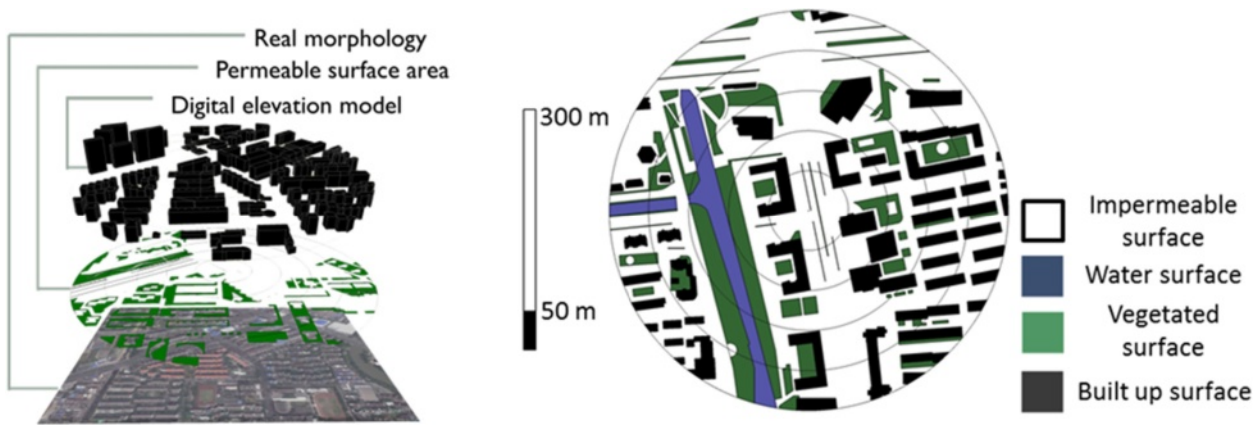

Fig. 4 Digital elevation models and land cover have been built upon the aerial image (Left). Four main land surface types have been identified in the five concentric annular areas with the sensor located at the centre of a disk of 250 m radius (Right)

Fig. 5 The nine studied urban units classified into LCZ5 (locations, marked with blue bullet points) in Hangzhou (Left). (Note: The Mantou Mountain, National Principle Weather station's location (reference, typical meteorological year file source) is marked as NP). An example of the land cover analysis is shown for Site 2 (Right; radius 250 m). Buildings are marked with black and vegetation with green

pervious, impervious and building footprint surface area ratios. The morphology characteristics of each annular area are based on the median value observations from the statistical analysis for the nine LCZ5 urban units (Table 3). The median was preferred over the mean because it is not affected by extremely low or high values and the calculated distributions were rather skewed than normal.

In idealised models building geometry is usually substituted with arrays of cubes. Common methods use cubes in staggered or aligned arrays (eg [35], [39–42]). Cubes in regular arrays are spaced in repeated intervals equal at all directions to the cube's edge length (ie aspect ratio = 1) (1 in Table 4). In this study however, the generic "urban unit model" comprises of square based boxes (ie blocks) with a non-uniform height in a staggered irregular array (3 in Table 4).

The staggered block array (3 in Table 4) has a north–south orientation. Each block has a base equal to the computational grid cells' horizontal dimensions. For example, the minimum building footprint area in this study was 64 m^2 because the computational grid cells had horizontal dimensions of 8 m (x) x 8 m (y). Regarding the vertical grid dimension (z), any buildings and vegetation in the urban unit model had a minimum height equal to the height of the first vertical grid cell (ie 0.50 m). Each block can represent a building (black), vegetated surface (green, grass or tree) or water surface (blue, zero height). The residual space between the

Table 2 Analysis of the morphological parameters for each annular area for a site with a LCZ5 classification (site 2 in Fig. 5)

Site 2.

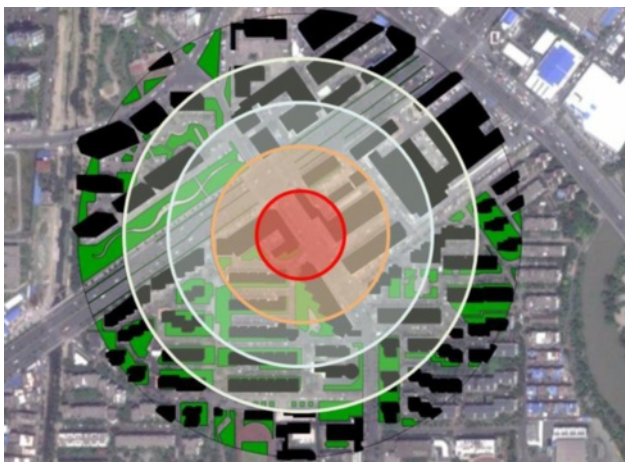

R-r (m)	P_r	I_r	F_r	z_0	$\sigma_H/\bar{H}$
0–50 (red)	0.05	0.64	0.31	1.5	0.52
50–100 (orange)	0.11	0.62	0.27	1.3	0.45
100–150 (blue)	0.17	0.56	0.27	1.2	1.08
150–200 (green)	0.16	0.60	0.24	1.7	0.99
200–250 (outer)	0.19	0.56	0.25	2.1	0.87

P_r pervious surface fraction, I_r impervious surface fraction, F_r building surface fraction, z_0 roughness length, $\sigma_H/\bar{H}$ standard deviation of the building height adjusted for the area weighted average height

Table 3 The median and the range (in brackets) of the key morphological parameters (10th to 90th centile) for the nine LCZ5 urban units shown in Fig. 5

Annulus R-r (m)	$\bar{H}$ (m)	P_r (%)	I_r (%)	λ_f (%)	F_r (%)	d (m)	z_0 (m)
0–50	20 (15–22)	7 (0–15)	72 (50–85)	17 (7–25)	21 (7–30)	6.7 (3.6–11.1)	1.8 (1.3–4)
50–100	18 (13–25)	11 (0–17)	61 (54–70)	15 (6–20)	27 (8–40)	8.9 (3.6–12.9)	1.4 (0.5–3)
100–150	20 (13–24)	15 (0–25)	65 (56–70)	13 (6–20)	23 (4–30)	7.6 (2.0–10.6)	1.8 (0.5–3)
150–200	17 (12–20)	15 (5–25)	60 (50–66)	14 (10–17)	24 (19–28)	8.6 (5.5–9.7)	1.2 (0.7–2)
200–250	19 (16–24)	15 (12–25)	56 (54–66)	13 (10–20)	23 (16–27)	8.3 (5.8–11.3)	1.8 (0.7–3)

(R-r refers to the inner and outer radius of the annuli borders)
$\bar{H}$ building footprint-area-weighted average height, P_r pervious surface fraction, I_r impervious surface fraction, λ_f frontal area ratio, F_r building surface fraction, d zero plane displacement height, z_0 roughness length

blocks represents the impervious surface (grey, eg roads, paved areas) (Fig. 4, right). The distance between the building blocks in each annular area is random and the number of the blocks representing buildings and vegetation was defined by the estimated F_r and P_r ratios respectively. The distribution of the blocks in each annular area is similar in all notional quarter annuli (ie 1/4th of the total annular area). The changes to the packing density and distance between the blocks produced a randomly dispersed layout that is expected to better fit the high spatial inhomogeneity of real cities than a regular staggered cube array.

Step 2. Normalisation of the reference weather data with the local UHI patterns (local scale)

The reference weather station (official, NP in Fig. 5) for Hangzhou is located at Mantou Mountain (30.23 ° N, 120.17 ° E, at an elevation of 42 m). This weather station is the source of the typical meteorological year (TMY) files for Hangzhou and it reports data with Hangzhou international airport's reference code (ZSHC) and the code 584570 in the World Meteorological Organisation's (WMO) weather station list. The steps for the normalisation of the reference weather data are as follows:

(1)((A) in Fig. 6) - The global horizontal solar radiation (GHR) from the typical meteorological year (TMY) file (584570_CSWD) was used for creating three distinctive groups in order to account for different weather forcing in each month (Fig. 6). Group 1 represents days with overcast sky conditions and rain events. Group 2 represents days with clear skies and average or "highly likely" weather conditions for the month, while Group 3 represents rather warm/hot days with a clear sky (Fig. 6). The 25th and 75th centiles (1st and 3rd quartiles) of the GHR values were used as the cut off points for the categorisation of the hourly TMY data into the groups. Group 1 for a given month contains all the days in that month that have hourly GHR values equal to or less than the 25th centile GHR value for the respective hours (lowest 25 % of GHR values). Similarly, Group 2 contains all the days in a month with hourly GHR values within the interquartile range of the GHR data for the respective hours (50 % of GHR values).

Table 4 Common urban morphology representations and the idealised "urban unit model" in this study (3)

Idealised models used to represent urban morphology

(1) Uniform height and aspect ratio

(2) Variable height and aspect ratio

(3) Variable height, aspect ratio and shape of blocks plus water (blue) and vegetation (green) surfaces.

Models (1) and (2) in table were adapted from [42]

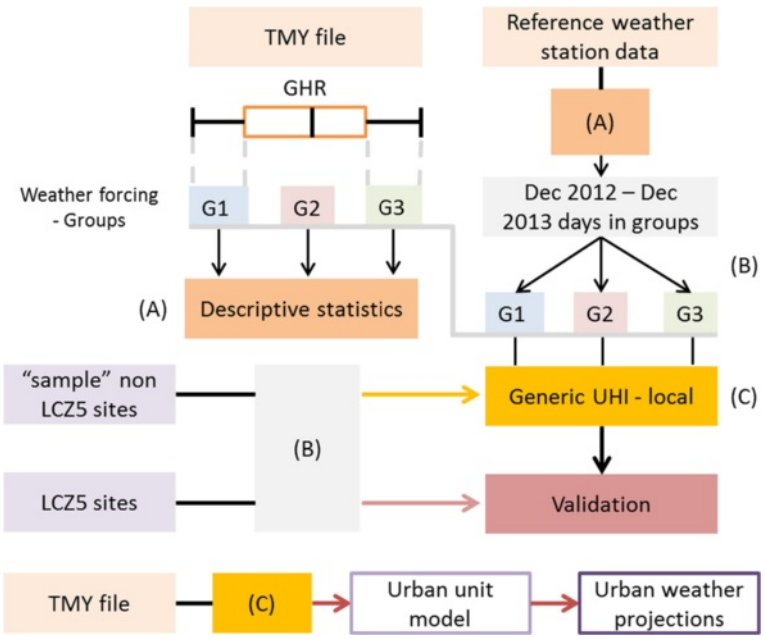

Fig. 6 Methodology flowchart of the model's validation and the generation of the adapted – "urbanised" weather dataset

Therefore, Group 2 is expected to be the most representative, "highly likely" weather forcing scenario. Group 3 contains days that had most of the hourly GHR values in the upper quartile (highest 25 % of GHR values). Here, the definition of "most of the hourly values" in this context relates to days with less than three hours with GHR values that do not fit into the specific group and where these hours are not between 12:00 and 16:00 h.

Following the grouping of the days, descriptive statistics were calculated for the daily mean air temperature, temperature range, daily mean RH and maximum temperature for all the days in each group. The remaining days from the TMY file that did not fit into any category were then distributed into either group 1, 2 or 3 according to their matches of daily mean air temperature, temperature range, daily mean RH and maximum temperature.

(2) ((B) in Fig. 6) - The descriptive statistics (ie mean T, T range, mean RH, max T) of (1) were also calculated for observations from the reference weather station (TMY source) for the period from December 2012 to December 2013 (Fig. 6). The results were then compared with the descriptive statistics ((A) in Fig. 6) of the weather forcing groups from the TMY data file as determined in (1). Following this, the individual days of the 2012–2013 observations from the reference weather station dataset were distributed into the monthly weather forcing groups according to the four criteria (ie mean T, T range, mean RH, max T from TMY data analysis) in descending order of weighting.

(3) ((C) in Fig. 6) - The data collected for each day from the sensors of the nine studied sites (LCZ5) highlighted in Fig. 5 as well as 10 additional ("sample") sites in Hangzhou (Fig. 7) were allocated to the weather forcing groups as defined in (2) ((B) in Fig. 6). Further to this, the observations from the 10 "sample" sites were used to create a generic hourly UHI pattern which relates to the difference of the sample sites' hourly average observations to the reference weather station data for each month and weather forcing group. The hourly average observations from the nine studied sites (LCZ5) were then used to validate this method. Here we are comparing real measurements of the 9 LCZ5 sites with the simulation results of the "urban unit model" forced with measured data from the reference (TMY source) weather station offset by the generic UHI effect as measured in the 10 "sample" sites.

(4) The normalisation of the TMY reference weather data with the generic UHI group patterns (T and RH offsets) was based on a simple offset of the hourly mean temperature and RH values for each weather forcing group (Eq. 1).

$$\mathrm{T(RH)urb}_{\mathrm{Group,hr}} = \mathrm{T(RH)ref}_{\mathrm{Group,hr}} + UHI(RH\ offset)_{Group,hr} \quad (1)$$

Where T(RH)urb is the air temperature (RH) after the adjustment to the hourly UHI (RH offset) pattern, T(RH)ref is the reference air temperature (RH) from the

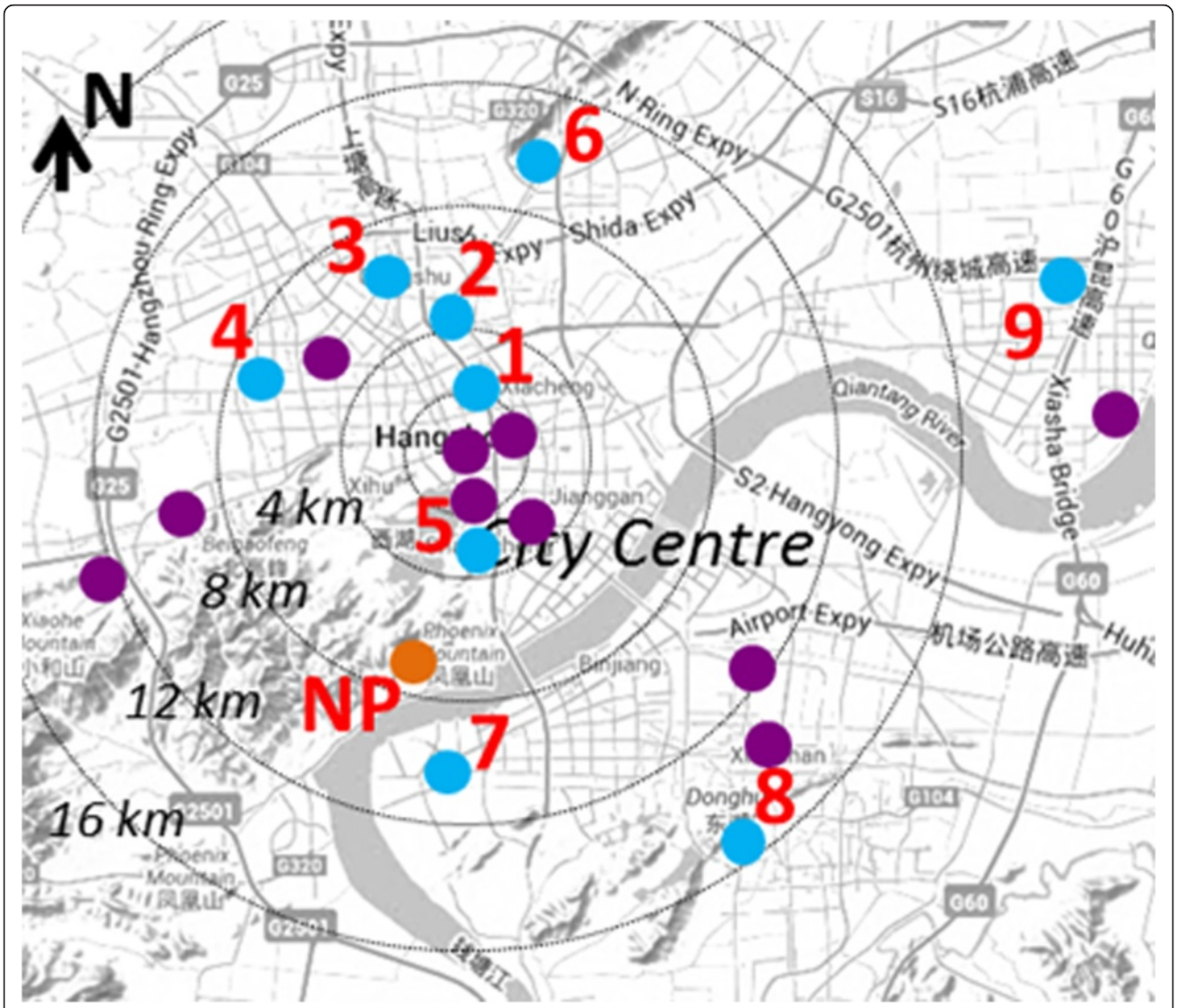

Fig. 7 Location of the 10 "sample" sites (purple bullet points) used for the assessment of generic UHI patterns in Hangzhou, China in relation to the 9 studied (LCZ5, blue bullet points) sites

TMY weather file and UHI (RH offset) is the positive or negative air temperature (RH) offset due to the urban heat island effect for each weather forcing group and hour respectively.

Step 3. Adaptation of the "localised" TMY data to include the effects of the site specific morphology (local scale + morphology = micro scale)

The idealised "urban unit model" (250 m radius) introduced above was implemented into micro-climatic simulations using a computational fluid dynamics – surface energy balance analysis tool (ENVI-met Version 4). In this final stage of data processing the hourly "localised" data generated according to methodology section (2) was used to initialise and force the hourly weather conditions in the simulation. The "urban weather projections" resulting from the simulations express the weather change at street level in relation to the baseline-reference weather (eg weather at airport sites or non-urban sites) caused by the effect of the site specific morphology in the city. These projections have the format of an additional hourly offset to the "localised" dataset for each weather forcing group.

ENVI-met is a three dimensional non-hydrostatic numerical micro-climatic model that couples an atmospheric, a soil and a one-dimensional (1-D) vegetation model and the surface energy balance. The atmospheric model is based on incompressible Reynolds averaged Navier Stokes (RANS) equations [43]. Wind speed and direction remain constant during the simulation. The effect of the surrounding urban environment on the turbulent kinetic energy and the turbulent energy dissipation rate were modelled using cyclic (periodic) lateral

and outflow boundary conditions (ie turbulence from last grid cells at outflow boundary are copied to the first grid cell at the inflow boundary) [43]. Air temperature (at 2 m above ground) and relative humidity at the inflow boundary were forced hourly with the "localised" air temperature and relative humidity TMY data for 24 h. The turbulence field was updated every 10 min; solar radiation was modelled with a dynamic time step (ie shorter when solar radiation is near its peak (1 s) and longer during morning and afternoon (2 s)); the internal temperature of buildings (free running) is calculated according to the heat transfer through walls and roofs, where all walls and roofs have the same thermal transmittance and albedo. The spin-up period was set to 4 h (starting at 20:00 on the day before the simulated day). The computational domain in ENVI-met comprises an equidistant grid that can be compressed or stretched in the vertical (z, height) dimension by using an expansion ratio but there is no option for the local refinement of the horizontal computational grid. The starting grid cell height, ie the height for the cell in contact with the ground surface, was set to 0.5 m and the grid remained equidistant below the height of 2.5 m with a grid cell spacing equal to dz = 0.5 m. The combination of a 0.5 m starting grid cell height with an 18 % grid height expansion ratio above 2.5 m resulted in a vertical grid with 16 grid cells at the lower part of the domain (ie the lower 20 m within the roughness sub-layer). The urban unit's 250 m radius resulted in 3D computational grids of 72 × 72 × 28 grid cells with a horizontal resolution of 8 m.

A sensitivity analysis of the simulation results showed that an increase of the horizontal resolution from 8 to 6 m and 3 m (Table 5) delivered no significant change in the model output. The coarsening ratio was not constant because of limitations set by the computational domain size and the fixed computational grid (ie the modelled geometry should fit to an integer number of grid cells). In addition, it was not possible to assess the grid sensitivity to computational grid dimensions below 3 m × 3 m due to the simulation domain size limitations (ie 250 × 250 grid cells maximum). That is because the urban unit has a diameter of 500 m and a number of grid cells in proximity to the domain borders must remain empty. Grid cell resolutions coarser than 8 m were not assessed because they were deemed too low for the purposes of this study.

Two scenarios were created for the assessment of the solution's sensitivity to the horizontal grid dimensions; one for winter that represents cold clear sky conditions and one for summer that represents hot weather with a clear sky in Hangzhou. The results from the case studies in both scenarios showed that the air temperature differences between the cases are less than 0.5 °C and for RH the difference was in the range of 2–3 % RH units.

The sensitivity to the vertical grid cell dimension was not assessed because it was considered important to a) have a solution at the height between 2.5 and 5 m above the ground (ie middle of grid cells, solution at 2.80, 3.44, 4.20 and 5.09 m) where the observations have been collected and b) have at least 10 grid cells in the lower 20 m of the domain and an expansion ratio below 20 % for the cells above the 20 m threshold.

In addition, two scenarios have been investigated for assessing the sensitivity of the model to the distribution and the amount of green-space in the model. The first scenario (Scenario 1) compared the air temperature at 3.5 m height above ground ($T_{3.5m}$) in Case 1, where the vegetation was distributed according to the statistical results from the land surface analysis, with Case 2, where all the vegetation surface area was moved to the centre of the urban unit and Case 3 where the vegetated area was moved towards the outer annuli (Fig. 8). The pervious surface area ratio (ie 0.15) remained the same for the urban unit model.

Scenario 2 compared the air temperature ($T_{3.5m}$) from Case 1 with 5 additional Cases (4 to 8) that had increasing ratios of pervious surface area that was distributed evenly (same percentage) in each annular area (Fig. 9). Each case had 5 % RH points more vegetated surface area (ie in the form of grass) than the previous one up to a maximum of P_r =0.4 which represents the upper limit for the "Local Climate Zone 5" classification.

The air temperature development in the idealised "urban unit" for both scenarios was simulated with ENVI-met (Version 4) for August 10, 2013 which represented a sunny hot day in Hangzhou. The sky was clear. The previous four days had been dry with 41 °C maximum air temperature and similar weather conditions as the day of the simulations. The analysis was conducted for 24 h from 00:00 China Standard Time (CST) to 23:00 CST.

Table 5 Case studies for the assessment of the solution's sensitivity to grid resolution

Case	Horizontal grid resolution (dx,dy) [m]	Vertical grid resolution (dz) [m]	Computational domain dimensions (x,y,z) [grid cells] (+no of nesting grids)	Coarsening ratio $r_{i,i+1}$
Case 1	(3, 3)	First 5 grid cells' height: 0.5 m, from 2.25 m to the top of the 3D domain: $dz_n = 1.18 \times dz_{n-1}$	207 × 207 × 28 (+6)	n.a.
Case 2	(6, 6)	Same as Case 1	104 × 104 × 28 (+5)	$r_{1,2} = 2.0$
Case 3	(8, 8)	Same as Case 1	72 × 72 × 28 (+4)	$r_{2,3} = 1.3$

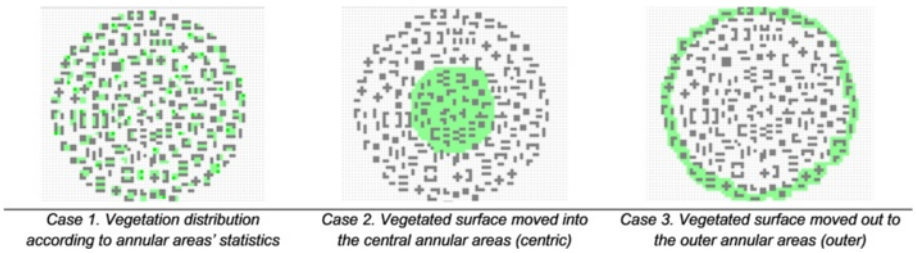

Fig. 8 Distribution of the vegetated surface area in the urban unit for the cases considered in Scenario 1 of the green-space sensitivity analysis

In both scenarios (green-space amount and distribution) the modelled temperature varied less than 0.5 °C between the cases showing that the solution is not sensitive to the distribution of the green-space in the model and the model performs as expected regarding the differences in the amount of vegetation.

Specifically, the assessment of the impact of the vegetation's location on the air temperature development in the urban canopy revealed that the proximity to "green" – vegetated space can decrease the urban heat island intensity during night-time and the maximum day-time air temperature. The marginal difference between the cases with a central allocation of the vegetated surface area and those were the vegetation was positioned at the outer border of the urban unit is an indication that the distance to a vegetated area is not enough to alone produce large cooling benefits during the day and attenuate the night-time urban heat island intensity. In Scenario 2 (amount of green-space), an increase to the urban unit's permeable surface area showed a small decrease in the average air temperature across the urban unit. The case with the largest vegetated surface area had the lowest daily air temperatures. A shift was noted in the air temperature distribution towards a higher occurrence frequency of temperatures at the cooler end. The differences between the cases were more evident in the average surface temperatures. The results suggest that high percentages of vegetated space can reduce the surface temperatures within the cities. There were, however, also strong indications that in places with a humid subtropical climate such as Hangzhou, in the case of successive hot, dry summer days, a reduction in soil water content will negate, to a large extent, the cooling benefits of the added vegetation.

In the Chinese building regulations Hangzhou is classified into the Hot Summer - Cold Winter climate zone [44]. In this zone, residential apartments are typically mixed mode with split air-conditioning and natural ventilation [45]. For the purpose of assessing the potential improvements in the estimation of building energy consumption against the "business as usual" case of using TMY data files the heating and cooling degree days were calculated and compared amongst the reference TMY file, the TMY file with a bulk hourly UHI offset and the "urbanised" TMY file after its adaptation to the "urban weather projections". The degree days have been calculated according to the data from the 584570_CSWD TMY file for Hangzhou at a base temperature of 18 °C [45] for heating and 26 °C [45] for cooling. The "urban unit model" methodology was validated for each of the 4 seasons and 3 different weather forcing conditions against the hourly average air temperature and RH observations from the 9 studied sites on a given day representative of the weather forcing conditions. The main parameters for the "urban unit model" validation are shown in Appendix 1. Looking at the dates given in Appendix 1 the "urban unit model" validation simulations were forced with the hourly weather data from the reference weather station (TMY source) overlaid with the representative urban heat island effect of the weather forcing group as calculated from the 10 "sample" sites' observations (and not the observed UHI during the

Scenario 2	pervious surface fraction P_r
Case 1	15%
Case 4	20%
Case 5	25%
Case 6	30%
Case 7	35%
Case 8	40%

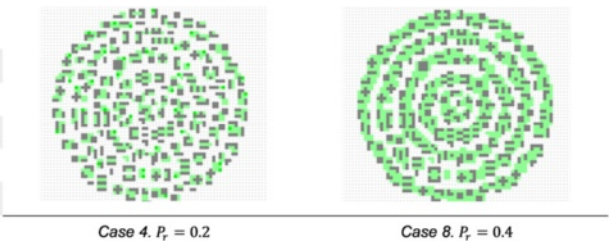

Fig. 9 The different percentages of vegetated surface area in the "urban unit" for the cases in Scenario 2 of the green-space sensitivity analysis. Top plan view of the computational domain (Right) for the cases with $P_r = 0.2$ and $P_r = 0.4$

simulated day) (see also Figs. 6 and 7). The hourly weather forcing for the "urban weather projections" simulations was undertaken with the hourly average air temperature and RH for the respective weather forcing group in the TMY file, adjusted by the representative bulk hourly UHI intensity (same as in the validation case) for the weather forcing groups.

Results and discussion of the "urban unit model" validation

This evaluation of the model's performance (Figs. 10, 11, 12 and 13) showed that urban micro-climatic simulations using the idealised "urban unit model" captures to within 1 °C the main characteristics of the diurnal air temperature development in all seasons.

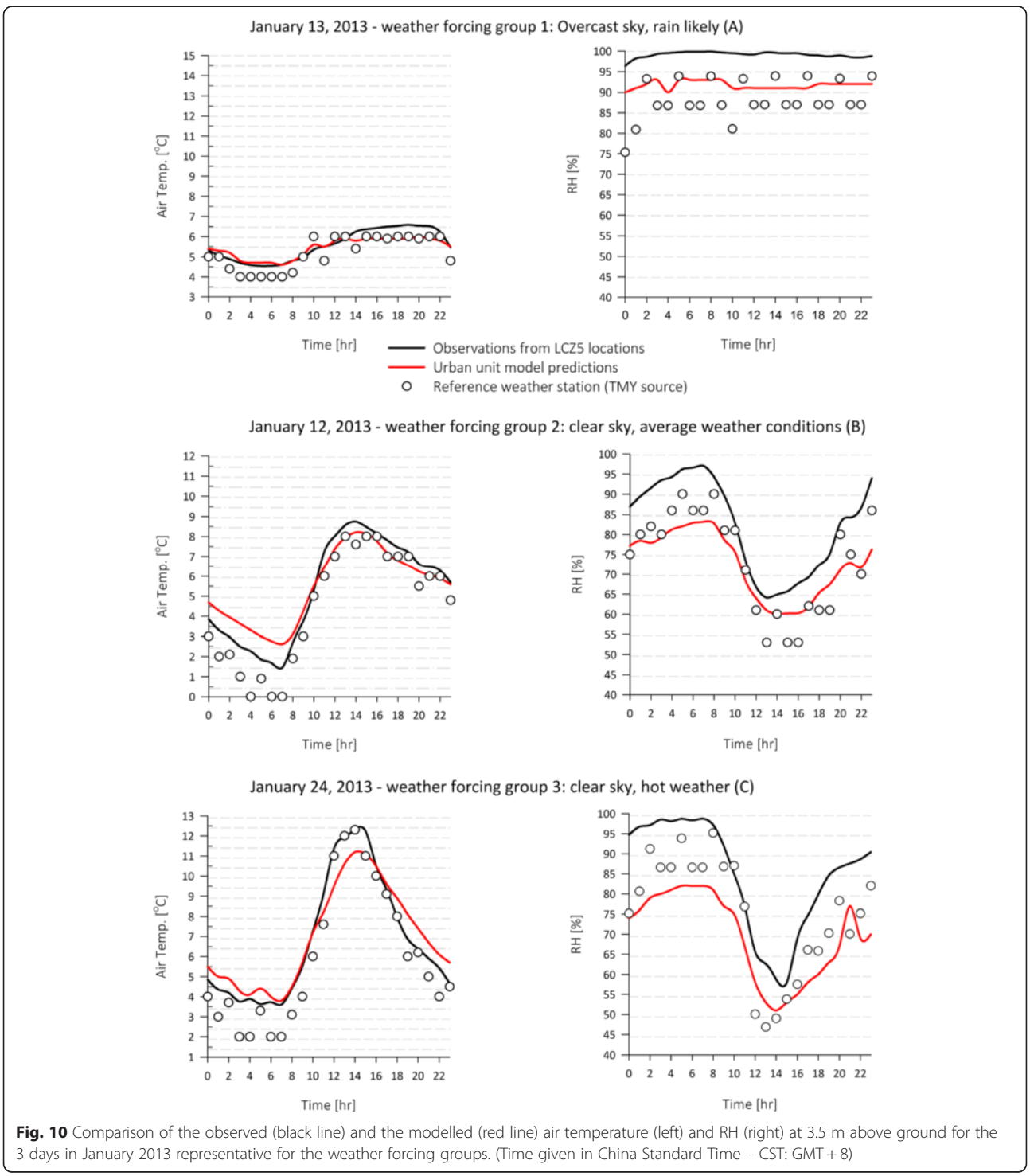

Fig. 10 Comparison of the observed (black line) and the modelled (red line) air temperature (left) and RH (right) at 3.5 m above ground for the 3 days in January 2013 representative for the weather forcing groups. (Time given in China Standard Time – CST: GMT + 8)

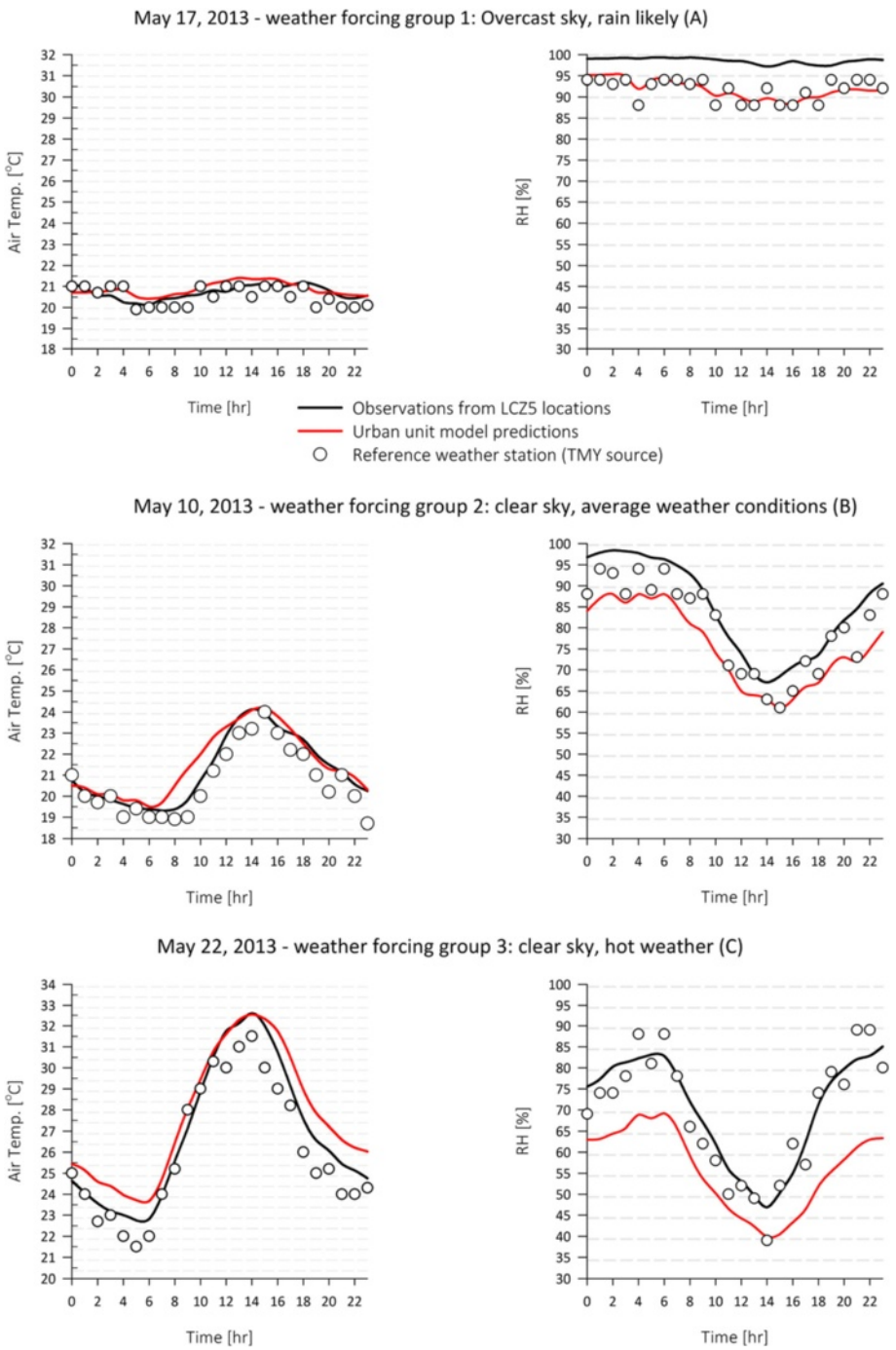

Fig. 11 Comparison of the observed (black line) and the modelled (red line) air temperature (left) and RH (right) at 3.5 m above ground for the 3 days in May 2013 representative for the weather forcing groups. (Time given in China Standard Time – CST: GMT + 8)

If the model output is a perfect prediction we would expect the observed temperatures (black line; average of hourly observations from the nine "LCZ5" sites, see Figs. 10, 11, 12 and 13) to be identical to the modelled temperatures (red line in Figs. 10, 11, 12 and 13). In this case the UHI effect experienced by the 9 LCZ5 sites and the 10 "sample" weather stations within the city would have to be identical. The ENVI-met model would have to perfectly forecast the average temperature/RH development at street level.

In the weather forcing group 1 winter scenario (January 13, 2013; Fig. 10 (top)) the modelled air temperature at 3.5 m above ground (Air Temp. [°C]; red line) is a very good fit to the observed temperature (black line; RMSE:

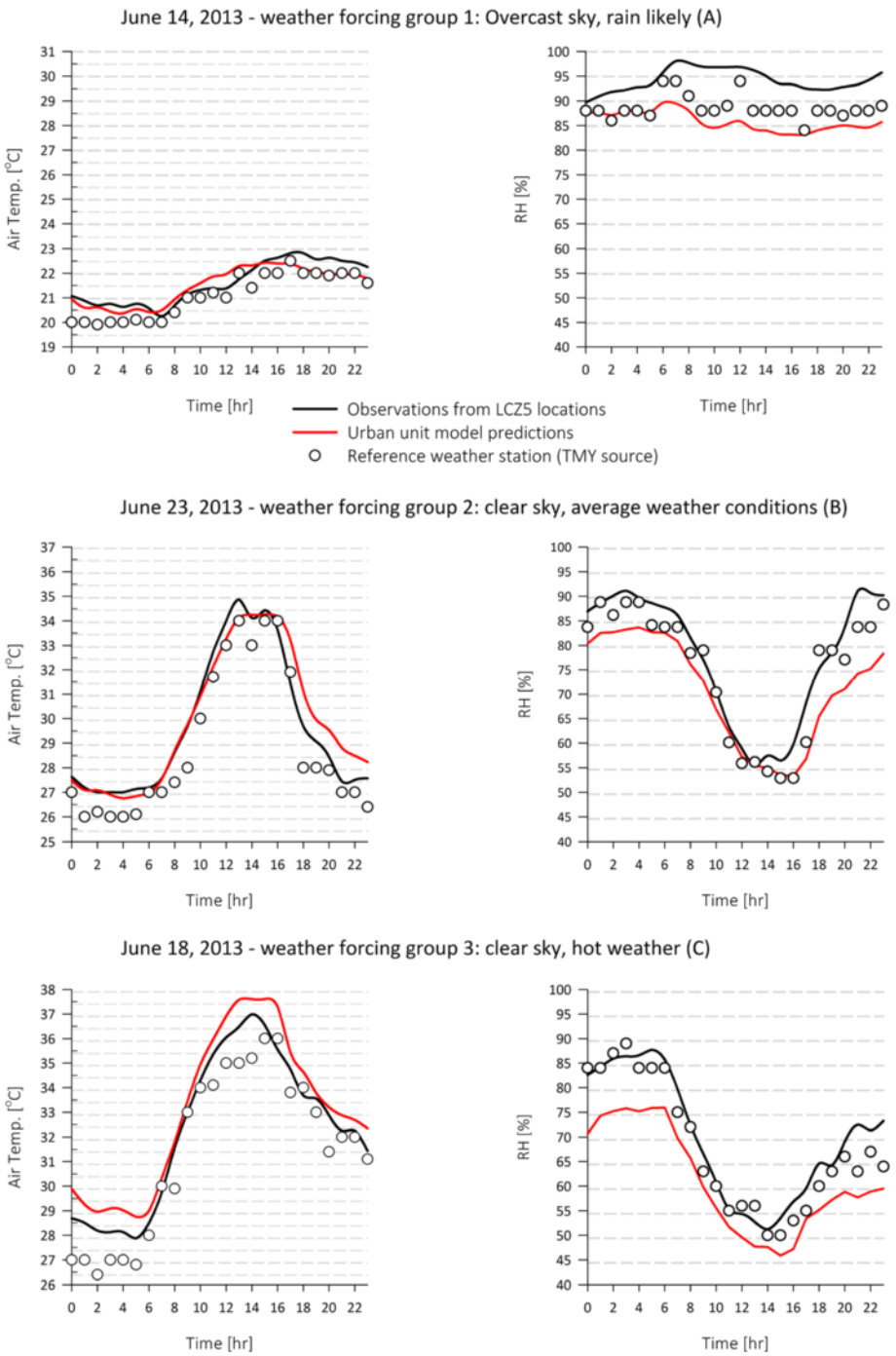

Fig. 12 Comparison of the observed (black line) and the modelled (red line) air temperature (left) and RH (right) at 3.5 m above ground for the 3 days in June 2013 representative for the weather forcing groups. (Time given in China Standard Time – CST: GMT + 8)

0.4, MAPE: 5 %, Table 6). The simulation results predict the night-time UHI better than the reference weather station (TMY source station) observations (circles in Figs. 10, 11, 12 and 13). The RH results (red line in Fig. 10 (right)) are representative of the observed RH diurnal trend. The simulated RH values are low compared to the average of the hourly observations but still represent an improvement in the urban weather conditions' prediction when compared to the reference weather station. In the case of weather forcing group 2 the simulated air temperature is a good fit to the observations for most hours of the day (Fig. 10 (middle)). The air temperature is overestimated early in the morning but the high values potentially better represent the urban conditions than the measured data

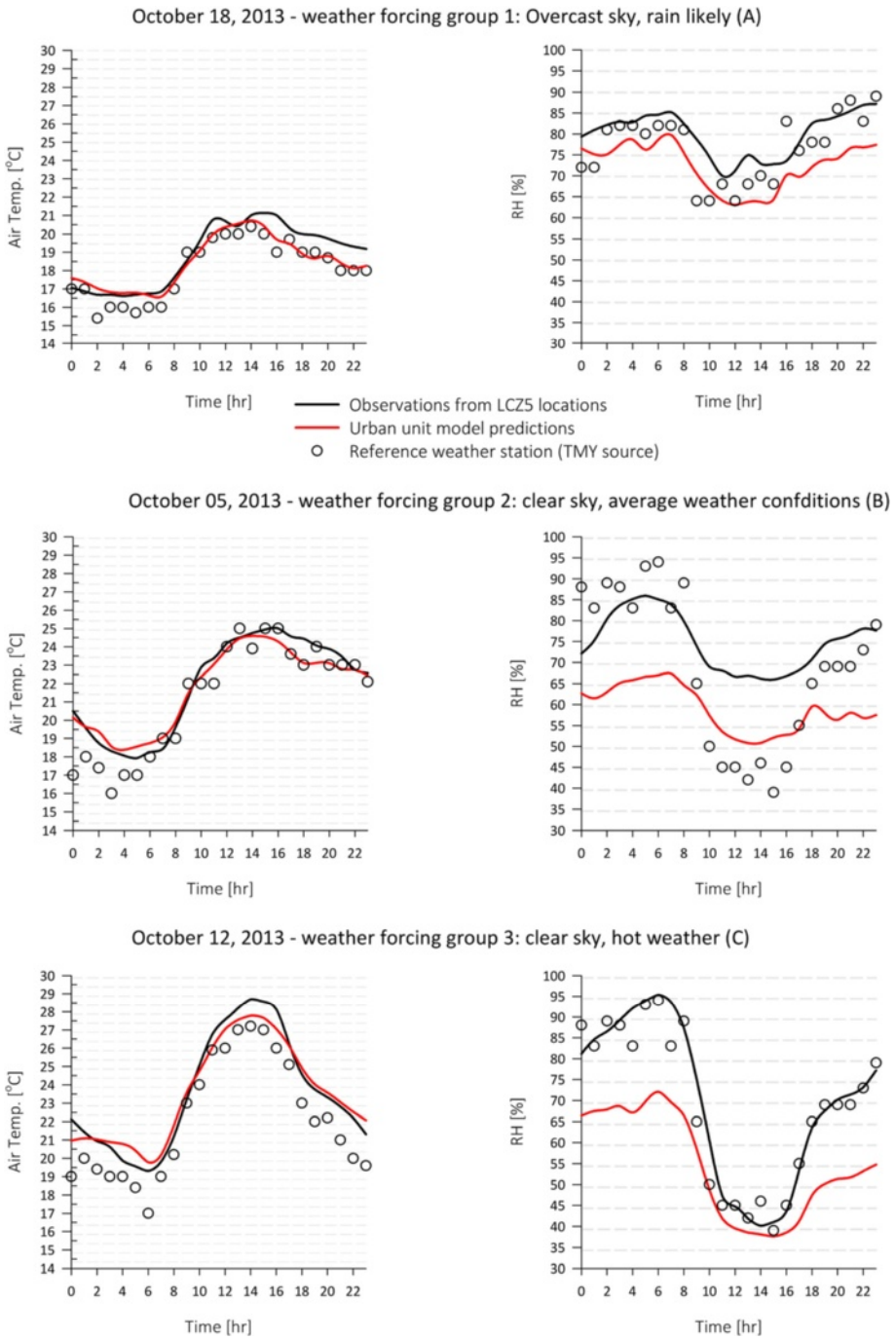

Fig. 13 Comparison of the observed (black line) and the modelled (red line) air temperature (left) and RH (right) at 3.5 m above ground for the 3 days in October 2013 representative for the weather forcing groups. (Time given in China Standard Time – CST: GMT + 8)

from the reference weather station. In the weather forcing group 3 case, winter daytime air temperatures are underestimated with the model failing to predict the temperature peak around 13:00 h. Nevertheless, the simulation results fit the observed data relatively well at night-time, in the early morning and afternoon. The failure to accurately predict the peak could be a result of an inaccurate representation of thermal mass and heat storage in the model [46] and the modelling of thermal diffusivity by ENVI-met [47].

The simulated RH in January for both the weather forcing group 2 and group 3 cases (Fig. 10), again replicates the daily observed trend and the RH predicted levels are comparable with the reference weather station observations

Table 6 Model performance indices determined for the winter and autumn simulations with the urban unit model

Model performance indices	T (RH) - winter (January)			T (RH) - autumn (October)		
	Group 1	Group 2	Group 3	Group 1	Group 2	Group 3
Mean Squared Error (MSE)	0.13 (56.1)	0.55 (116.1)	0.70 (258.5)	0.50 (61.6)	0.31 (261.2)	0.39 (287.1)
Mean Bias Error (MBE)	−0.14 (-7.4)	0.12 (-10)	0.16 (-15.4)	−0.42 (-7.5)	−0.17 (-15.9)	−0.02 (-15.3)
MSE systematic	0.11 (55.8)	0.49 (112.5)	0.40 (246.3)	0.33 (56.7)	0.22 (255.4)	0.23 (280.9)
Root Mean Squared Error (RMSE)	0.36 (7.50)	0.74 (10.75)	0.84 (16.05)	0.70 (7.85)	0.56 (16.16)	0.63 (16.95)
RMSE systematic	0.33 (7.47)	0.70 (10.61)	0.64 (15.70)	0.58 (7.53)	0.47 (15.98)	0.48 (16.76)
MSE unsystematic	0.02 (0.73)	0.05 (3.05)	0.30 (11.17)	0.17 (4.89)	0.09 (5.85)	0.16 (6.26)
RMSE unsystematic	0.15 (0.85)	0.23 (1.75)	0.55 (3.34)	0.41 (2.21)	0.31 (2.42)	0.40 (2.50)
Mean Absolute Percentage Error (MAPE)	5 % (8 %)	21 % (12 %)	11 % (18 %)	3 % (9 %)	2 % (21 %)	2 % (21 %)
Index of agreement d	0.92 (0.13)	0.97 (0.78)	0.98 (0.72)	0.95 (0.68)	0.99 (0.48)	0.99 (0.77)

(especially when considering the 5 % units RH sensor accuracy) for the largest part of the day.

The model underestimates the RH during early morning before 08:00 o'clock indicating a possible discrepancy between the modelled vegetation properties (ie amount and type of trees, grass) and reality. However, this difference is not expected to have a significant effect on the model's application because 1) the predicted RH values are relatively close to the reference weather station observations and 2) the largest discrepancy is early in the morning and late at night in winter when typically dehumidification is not an option when split AC units operate in heating mode (or auxiliary heating sources are used instead). The satisfactory prediction of the expected urban heat island during the night ($\Delta T_{Case\ -\ reference}$) in all three cases is a further indication that this level of inaccuracy is not detrimental to the overall function of the model.

In the spring scenario (May 2013, Fig. 11) the air temperature was overestimated during night and early morning. The simulated air temperature in the afternoon was representative of the observed air temperature across all three weather forcing groups. The reference weather station observations were consistently very close to the urban observations showing the existence of a rather small urban heat island effect in Hangzhou during spring. The RH in the urban unit model was again underestimated with the error being acceptable (RMSE: 7, MAPE: 7 %, Table 7) in the case that represents overcast sky conditions (group 1, Fig. 11 (top)) but significant (RMSE: 15, MAPE: 20 %, Table 7) in the weather forcing group 3 case (ie clear sky, hot weather). Overall, in the spring scenario the night-time urban heat island intensity was overestimated across all the weather forcing groups. However, in May night-time the air temperature is still low and the air-conditioning demand if any is expected to be minimal. In the weather forcing group 3 case (Fig. 11 (bottom)) the high air temperature at noon suggests that indoor temperatures are highly likely to exceed the comfort band threshold of 27 °C [48] creating a demand for cooling. The simulated air temperature peaks are a good fit to the urban observations and in most cases they represent the urban weather development better than the reference weather station measurements.

In the summer scenario (June, Fig. 12), the air temperature predictions from all three weather forcing groups fit the observations from the studied LCZ5 sites

Table 7 Model performance indices determined for the spring and summer simulations with the urban unit model

Model performance indices	T (RH) - spring (May)			T (RH) - summer (June)		
	Group 1	Group 2	Group 3	Group 1	Group 2	Group 3
Mean Squared Error (MSE)	0.08 (48.5)	0.31 (91.3)	0.90 (226.5)	0.15 (77.2)	0.52 (65.2)	0.67 (88.3)
Mean Bias Error (MBE)	0.15 (-6.8)	0.31 (-9.2)	0.84 (-14.4)	−0.11 (-8.4)	0.23 (-6.9)	0.75 (-8.9)
MSE systematic	0.04 (46)	0.11 (89.8)	0.80 (219.4)	0.04 (73.5)	0.08 (53.6)	0.56 (84.0)
Root Mean Squared Error (RMSE)	0.29 (6.9)	0.56 (9.6)	0.95 (15.1)	0.38 (8.8)	0.72 (8.1)	0.82 (9.4)
RMSE systematic	0.19 (6.78)	0.33 (9.47)	0.89 (14.81)	0.20 (8.56)	0.27 (7.32)	0.75 (9.17)
MSE unsystematic	0.05 (1.96)	0.20 (2.45)	0.10 (8.37)	0.11 (3.71)	0.45 (11.60)	0.11 (4.73)
RMSE unsystematic	0.22 (1.40)	0.45 (1.57)	0.32 (2.89)	0.33 (1.93)	0.67 (3.41)	0.33 (2.17)
Mean Absolute Percentage Error (MAPE)	1 % (7 %)	2 % (11 %)	3 % (20 %)	2 % (9 %)	2 % (9 %)	2 % (13 %)
Index of agreement d	0.78 (0.17)	0.97 (0.82)	0.98 (0.73)	0.94 (0.29)	0.98 (0.89)	0.98 (0.85)

reasonably well (RMSE: 0.4 to 0.8, MAPE: 2 %, Table 7). In June 2013, in the weather forcing group 3 case, the air temperature is over predicted at noon and early morning. This recurring pattern in the simulation of hot weather conditions in spring and summer can be the result of underrepresentation of the permeable surface and soil water content in the model [47]. The RH simulation results support this argument with the error of the simulated RH in morning being in the range of 15 RH percentage units.

Overall, the RH is underestimated during large parts of the day but the simulated RH levels are comparably close to the observations with a RMSE around 10 RH units and MAPE of 10 % (Table 7).

In October (autumn, Fig.13) the model simulates the urban heat island development during the night with the simulated air temperature being close to the observations from the LCZ5 sites. The modelled air temperature development is more realistic for the urban environment than the measured reference temperature. At noon and under hot weather conditions (weather forcing group 3), the model fails to accurately predict the peak but the simulated temperature is still an improvement in comparison with the reference air temperature observations. In general, domestic buildings in October are expected to be free-running (no heating or cooling). There is a small demand for cooling in September and for heating from mid-November onwards. The validation of the model showed that cooling demand in autumn is likely to be under estimated at noon and in the early afternoon but its prediction is largely improved at night when the air temperature simulation results fit the urban observations very well (RMSE: 0.6 to 0.7, MAPE: ~2 %, Table 6). The simulated RH follows the observed diurnal RH trend but in weather forcing groups 2 and 3 the error is large with the RMSE equal to 16 and 17 RH % units respectively and the MAPE in the range of 20 %.

This discrepancy might be a result of weather events that ENVI-met cannot simulate such as mist, haze and rain. Specifically on the 12th of October there was mist until 08:00 in the morning when it dispersed and at the same time the model's prediction accuracy increased. In the evening the large error in the RH prediction can be attributed to the modelled soil water content and the position of some of the LCZ5 sites being close to large water bodies. In late autumn the RH plays little role as there is no dehumidification load associated with heating. In addition, the largest RH error in October was noticed early in the morning and during the evening when the temperature is expected to be within the comfort band of the thermostatic set points and there will be no cooling requirement.

Overall, the accuracy of the model can be viewed as satisfactory in relation to its purpose, considering the uncertainties involved in the initialisation of the model and the simulation itself. Furthermore, the model performance evaluation indices' scores for air temperature (Tables 6 and 7) are comparable to other published work [46, 49]. The index of agreement d takes values in the range {0, 1} with a value of 1 indicating a perfect match between the model prediction and the observations [46, 50]. The index of agreement scores low in the weather forcing group 1 results for all seasons. However the Mean Absolute Percentage Error of the air temperature was consistently less than 10 % in almost all cases and the systematic component of the root mean square error (RMSEs) was lower than 0.5 °C in most cases and always lower than 1 °C. The systematic component of the error (ie RMSEs), which represents the error attributed to the simulation and the error integrated into the initialisation estimates, should approach 0 [46]. The unsystematic component should approach the value of RMSE [50]. The relatively low RMSE values in conjunction with the fact that the model results were closer to the urban observations than the reference measured values show that the model's performance is acceptable.

The accuracy of the RH prediction is most important during the cooling season when dehumidification is required. In Hangzhou and other similar cities with a humid sub-tropical climate the full cooling season is expected to last from June to September [31, 51]. The validation showed that in June and for the summer scenario the error is below 10 RH percentage units. However, the measured RH from the reference weather station fits better to the urban observations than the simulated RH. Furthermore there is only a marginal RH difference between the urban and the reference sites. Therefore, the urban weather projections were used to adapt the air temperature only in the TMY file and not the relative humidity.

A full scale error analysis was not undertaken due to lack of available data/input parameters notably the hourly global solar radiation and soil properties. The validation has been restricted to days that are typical for the weather forcing groups' conditions. The main sources of systematic error are the input initialisation parameters, in particular hourly global solar radiation. Other sources of systematic error include the initial boundary conditions, building and vegetation properties. Unsystematic errors might be a result of the thermal diffusivity [47] and turbulence modelling, the modelling of evapotranspiration and the total heat advection to the atmosphere.

Results and discussion of the TMY file for Hangzhou adapted with the urban unit model

Following the "urban unit model" validation the TMY file for Hangzhou (584570_CSWD) was adapted to

include the "urban weather projections" (UWP) according to the methods outlined above. A comparison amongst the reference TMY, the TMY overlaid with the bulk "city" UHI effect (TMY + UHI) and the micro-scale "urban weather projections" (TMY-UWP) is shown in Fig. 14. In the "TMY + UHI" HDD have decreased by 6 % from 1598 days in the reference TMY and in the "TMY-UWP" file by 13 % showing that the local specific micro-climate attributes an additional 7 % heating load reduction to the bulk UHI effect of the city. This difference between the "TMY-UWP" and the "TMY + UHI" files is a reflection of the thermal characteristics of the specific urban morphology of the studied sites compared to the wider city. CDD in the "TMY + UHI" file are 17 % more than the reference TMY file (207 days). The "TMY-UWP" file shows an additional 14 % increase in comparison with the "TMY + UHI" file.

The impact of the change in HDD and CDD was assessed in terms of heating and cooling loads for a domestic and a non-domestic building scenario in Hangzhou. For this purpose, the "urbanised" (TMY-UWP) and the reference TMY files were used within a dynamic thermal simulation tool (TRNSYS Version 17.1) to model the annual heating and cooling load for both scenarios. The calculated heating and cooling loads for both the domestic and the non-domestic building case show that the energy performance simulations with the reference TMY file result in an approximate 20 % over prediction of the heating load and 20 % under prediction of the cooling load demand in comparison with the simulation results with the use of the TMY-UWP file.

Conclusions

The validation of the "urban unit model" and the results of its implementation into micro-climatic simulations show that there is a potential for the simplification of urban site modelling and for the wider application of the method introduced in this paper as a tool for adapting typical meteorological weather data files to represent the neighbourhood scale of cities with a humid sub-tropical climate.

Overall, the comparison amongst the reference (ie 1598 HDD), a bulk "city" UHI effect and the adapted for the "urban weather projections" TMY files indicates that there was a 6 % decrease in HDD that is attributed to the bulk "city" UHI effect and an additional 7 % (ie from 6 to 13 %) that can be directly attributed to the local specific urban morphology of the 9 LCZ5 sites. The total increase of CDD from the reference (ie 207 CDD) to the "urban weather projections" TMY files is in the range of 30 %. This assessment indicates that cooling loads can be significantly underestimated in the business as usual case of using the reference TMY file and that the urban effect on air temperature should not be neglected.

The heating and cooling demand has been further calculated for a domestic and a non-domestic building case in Hangzhou. It has been observed that in both cases there is an approximate 20 % increase of the cooling load and a 20 % decrease of the heating load. If typical COP values for a reversible air-

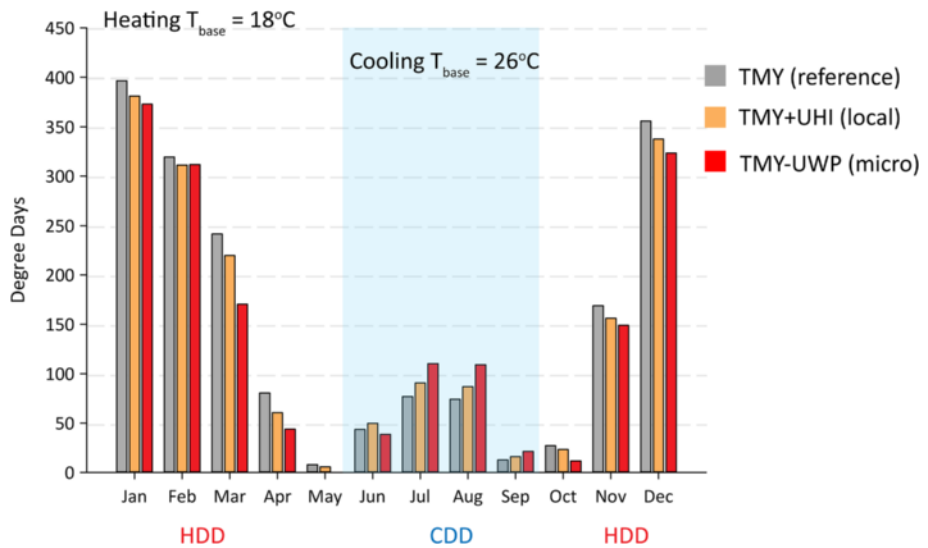

Fig. 14 Comparison of the degree days in the reference TMY (TMY reference, gray; 1598 HDD, 207 CDD) with the TMY overlaid with the bulk "city" UHI effect (TMY + UHI, orange; 1495 HDD, 243 CDD) and the micro-scale "urban weather projections" (TMY-UWP, red; 1383 HDD, 279 CDD). T_{base} is the temperature threshold used for the calculation of the HDD and CDD. The area with the light blue background marks the cooling period

conditioning system are taken as 2.0 for heating and 3.5 for cooling then the total electricity consumption estimated with the use of the "urban weather projections" TMY file will be decreased by 11 % in comparison with the "business as usual" (ie reference TMY) case. This is an interesting result showing the impact highly efficient heat pumps and air-conditioning systems can have on the electricity consumption of cities with a humid sub-tropical climate. However, this assumes a cooling set-point of 26 °C. If a lower set-point is used the predicted energy savings will be lost.

In the majority of cases it would be difficult to justify the additional level of analysis described here to develop the localised weather data file over the generic bulk "city" UHI file. The method is shown to deliver an enhancement which in large developments could be justified. Single, smaller/residential buildings can take the bulk UHI correction approach. This methodology would also benefit initial stages of urban planning and could inform decisions on the use and the urban form of existing and new developments in the city.

Future work is looking to expand this methodology to different urban morphologies and to transfer it to different climates.

Appendix 1

Table 8 Main input parameters for the simulations with the urban unit model in January 2013

Input parameter	Jan 13, 2013	Jan 12, 2013	Jan 24, 2013	Source
Weather forcing Group	Group 1	Group 2	Group 3	
Specific humidity 2500 m (750 mbar) *gr w/kg dry air*	3.3	2.0	1.1	[52]
Prevalent wind direction (N = 0 clockwise)	22	225	225	[53]
Wind speed 10 m ab. gr. *m/s*	3.2	2.1	2.5	[53]
Roughness length z_0	0.1	0.1	0.1	[36]
Mean wall albedo	0.23	0.23	0.23	[49]
Mean roof albedo	0.50	0.50	0.50	
Wall heat transmittance $W.\ m^{-2}.\ K^{-1}$	1.4	1.4	1.4	
Roof heat transmittance $W.\ m^{-2}.\ K^{-1}$	0.9	0.9	0.9	
Underground soil temperature (Upper-Middle-Deep layer) *K*	278.4	277.3	280.6	[52]
	279.6	279.5	281.4	
	282.6	283.0	282.4	
Underground soil humidity (Upper-Middle-Deep layer)	38 %	36 %	34 %	[52]
	38 %	36 %	35 %	
	36 %	35 %	35 %	

Table 9 Main input parameters for the simulations with the urban unit model in June 2013

Input parameter	Jun 14, 2013	Jun 23, 2013	Jun 18, 2013	Source
Weather forcing Group	Group 1	Group 2	Group 3	
Specific humidity 2500 m (750 mbar) *gr w/kg dry air*	8.9	12	11.3	[52]
Prevalent wind direction (N = 0 clockwise)	45	90	225	[53]
Wind speed 10 m ab. gr. *m/s*	3.1	2.8	3.1	[53]
Roughness length z_0	0.1	0.1	0.1	[36]
Mean wall albedo	0.23	0.23	0.23	[49]
Mean roof albedo	0.50	0.50	0.50	
Wall heat transmittance $W.\ m^{-2}.\ K^{-1}$	1.4	1.4	1.4	
Roof heat transmittance $W.\ m^{-2}.\ K^{-1}$	0.9	0.9	0.9	
Underground soil temperature (Upper-Middle-Deep layer) *K*	294.3	299	300	[52]
	292.7	294	293	
	290.6	291	291	
Underground soil humidity (Upper-Middle-Deep layer)	38 %	39 %	38 %	[52]
	38 %	37 %	38 %	
	37 %	36 %	37 %	

Table 10 Main input parameters for the simulations with the urban unit model in May 2013

Input parameter	May 17, 2013	May 10, 2013	May 22, 2013	Source
Weather forcing Group	Group 1	Group 2	Group 3	
Specific humidity 2500 m (750 mbar) *gr w/kg dry air*	8.3	7.2	3.9	[52]
Prevalent wind direction (N = 0 clockwise)	0	110	0	[53]
Wind speed 10 m ab. gr. *m/s*	1.6	2.8	2.8	[53]
Roughness length z_0	0.1	0.1	0.1	[36]
Mean wall albedo	0.23	0.23	0.23	[49]
Mean roof albedo	0.50	0.50	0.50	
Wall heat transmittance $W.\ m^{-2}.\ K^{-1}$	1.4	1.4	1.4	
Roof heat transmittance $W.\ m^{-2}.\ K^{-1}$	0.9	0.9	0.9	
Underground soil temperature (Upper-Middle-Deep layer) *K*	292.7	293.2	296.0	[52]
	290.3	288.9	291.0	
	288.0	287.2	288.0	
Underground soil humidity (Upper-Middle-Deep layer)	35 %	37 %	33 %	[52]
	35 %	37 %	34 %	
	34 %	35 %	34 %	

Table 11 Main input parameters for the simulations with the urban unit model in October 2013

Input parameter	October 18, 2013	October 05, 2013	October 12, 2013	Source
Weather forcing Group	Group 1	Group 2	Group 3	
Specific humidity 2500 m (750 mbar) *gr w/kg dry air*	5.3	0.6	0.8	[52]
Prevalent wind direction (N = 0 clockwise)	0	225	200	[53]
Wind speed 10 m ab. gr. *m/s*	3.0	2.5	2.2	[53]
Roughness length z_0	0.1	0.1	0.1	[36]
Mean wall albedo	0.23	0.23	0.23	[49]
Mean roof albedo	0.50	0.50	0.50	
Wall heat transmittance $W.\ m^{-2}.\ K^{-1}$	1.4	1.4	1.4	
Roof heat transmittance $W.\ m^{-2}.\ K^{-1}$	0.9	0.9	0.9	
Underground soil temperature (Upper-Middle-Deep layer) *K*	291.0	291.3	292.5	[52]
	293.1	292.8	291.3	
	294.1	294.0	293.1	
Underground soil humidity (Upper-Middle-Deep layer)	33 %	32 %	29 %	[52]
	34 %	33 %	32 %	
	34 %	33 %	32 %	

Abbreviations

CDD, cooling degree day; CDH, Ccooling degree hour; CST, China standard time; GHR, global horizontal radiation; GMT, Greenwich mean time; HDD, heating degree Dday; HDH, heating degree hour; HVAC, heating, ventilation and air conditioning; LCZ, local climate zone; MAPE, mean absolute percentage error; MBE, mean bias error; MSE, mean squared error; RANS, Reynolds averaged Navier stokes; RH, relative humidity; RMSE, root mean squared error; TKE, turbulent kinetic energy; TMY, typical meteorological year; UHI, urban heat island; UWP, urban weather projections

Acknowledgement

This work is part of the activities of the University of Southampton's Energy and Climate Change Division and the Sustainable Energy Research Group (www.energy.soton.ac.uk) on cities and infrastructure. It is partly supported by the EPSRC Grant EP/J017698/1, "Transforming the Engineering of Cities to Deliver Societal and Planetary Wellbeing" and EP/K012347/1, "International Centre for Infrastructure Futures (ICIF)". The installation work of the sensors' network in Hangzhou and Ningbo is supported by the Ningbo Natural Science Foundation (No. 2012A610173) and the Ningbo Housing and Urban-Rural Development Committee (No. 201206).

Authors' contributions

LB developed the methodology, the "urban unit model" and managed the work in this study. PABJ provided guidance, reviewed and supervised all stages of this study. ABSB contributed to the management of this study and reviewed the final outcome. MFJ contributed to the development of the initial idea for this study and reviewed parts of the work and the final outcome. TS installed and managed the sensors network in China, collected the observations and contributed to their analysis. DHCC contributed to the development of the sensors network in China and supervised the data analysis. JD contributed to the management of the sensors network and reviewed the data analysis and parts of this study. All authors read and approved the final manuscript.

Competing interests

The authors declare that they have no competing interests.

Author details

[1]Energy & Climate Change Division, Sustainable Energy Research Group (SERG), Faculty of Engineering and the Environment, University of Southampton, Southampton SO17 1BJ, UK. [2]Urban Energy Systems, Faculty of Civil Engineering, Bauhaus-Universität Weimar, Weimar, Germany. [3]Centre for Sustainable Energy Technologies (CSET), University of Nottingham Ningbo, Ningbo, People's Republic of China. [4]School of Architecture, Faculty of Humanities and Social Sciences, University of Liverpool, Liverpool, UK. [5]Faculty of Engineering, University of Nottingham, Nottingham, UK.

Received: 2 February 2016 Accepted: 30 June 2016
Published online: 08 July 2016

References

1. Crawley DB (1998) Which weather data should you use for energy simulations of commercial buildings? In: ASHRAE Transactions. ASHRAE, Atlanta, USA, pp 498–515
2. Hacker J, Capon R, Mylona A (2009) Use of climate change scenarios for building simulation: the CIBSE future weather years. The Chartered Institution of Building Services Engineers, London, UK
3. Thomas PC, Moller S (2006) HVAC system size - getting it right. In: Clients Driving Innovation: Moving Ideas into Practice. Cooperative Research Centre for Construction Innovation, Brisbane, Australia
4. Burdick A (2011) Strategy Guideline: Accurate heating and cooling load calculations. Oak Ridge, USA.
5. US Department of Energy (2016) EnergyPlus - Weather Data Sources. Available via https://energyplus.net/weather/sources. Accessed 19 June 2016
6. Mylona A (2012) The use of UKCP09 to produce weather files for building simulation. Build Serv Eng Res Technol 33(1):51–62
7. Oke TR (1982) The energetic basis of the urban heat island. Q J R Meteorol Soc 108(455):1–24
8. Collier CG (2006) The impact of urban areas on weather. Q J R Meteorol Soc 132(614):1–25
9. Taha H, Konopacki S, Gabersek S (1999) Impacts of Large-Scale Surface Modifications on Meteorological Conditions and Energy Use: A 10-Region Modeling Study. Theor Appl Climatol 62(3):175–185
10. Memon RA, Leung DYC, Liu CH (2009) An investigation of urban heat island intensity (UHII) as an indicator of urban heating. Atmos Res 94(3):491–500
11. Jusuf ST, Wong NH (2009) Development of empirical models for an estate level air temperature prediction in Singapore. Paper presented at 7th International Conference on Urban Climate. June 29 - July 3, Yokohama, Japan.
12. Kolokotroni M, Davies M, Croxford B, Bhuiyan S, Mavrogianni A (2010) A validated methodology for the prediction of heating and cooling energy demand for buildings within the Urban Heat Island: Case-study of London. Sol Energy 84(12):2246–2255
13. Kolokotroni M, Ren X, Davies M, Mavrogianni A (2012) London's urban heat island: Impact on current and future energy consumption in office buildings. Energy Buildings 47:302–311
14. Chan ALS (2011) Developing a modified typical meteorological year weather file for Hong Kong taking into account the urban heat island effect. Build Environ 46(12):2434–2441
15. Wong NH, Jusuf ST, Tan CL (2011) Integrated urban microclimate assessment method as a sustainable urban development and urban design tool. Landsc Urban Plan 100:386–389
16. Watkins R, Palmer J, Kolokotroni M, Littlefair P (2002) The London heat island: results from summertime monitoring. Build Serv Eng Res Technol 23(2):97–106
17. Kershaw T, Sanderson M, Coley D, Eames M (2010) Estimation of the urban heat island for UK climate change projections. Build Serv Eng Res Technol 31(3):251–263
18. De La Flor FS, Domínguez SA (2004) Modelling microclimate in urban environments and assessing its influence on the performance of surrounding buildings. Energy Buildings 36(5):403–413
19. Chen F, Kusaka H, Bornstein R, Ching J, Grimmond CSB, Grossman-Clarke S, Loridan T, Manning KW, Martilli A, Miao S, Sailor D, Salamanca FP, Taha H, Tewari M, Wang X, Wyszogrodzki AA, Zhang C (2011) The integrated WRF/urban modelling system: development, evaluation, and applications to urban environmental problems. Int J Climatol 31(2):273–288

20. Yamada T, Koike K (2011) Downscaling mesoscale meteorological models for computational wind engineering applications. J Wind Eng Ind Aerodyn 99(4):199–216
21. Tewari M, Kusaka H, Chen F, Coirier WJ, Kim S, Wyszogrodzki AA, Warner TT (2010) Impact of coupling a microscale computational fluid dynamics model with a mesoscale model on urban scale contaminant transport and dispersion. Atmos Res 96(4):656–664
22. Schlünzen KH (2010) Joint modelling of obstacle induced and mesoscale changes-current limits and challenges. Paper presented at The Fifth International Symposium on Computational Wind Engineering (CWE2010). May 23-27, 2010, Chapel Hill, North Carolina, USA.
23. Baklanov A, Martilli A, Grimmond CSB, Mahura A, Ching J, Calmet I, Clark P, Esau I, Dandou A, Zilitinkevich S, Best MJ, Mestayer P, Santiago JL, Tombrou M, Petersen C, Porson A, Salamanca F, Amstrup B (2010) Hierarchy of Urban Canopy Parameterisations for different scale models. MEGAPOLI Project Scientific Report 10-04. Danish Meteorological Institute, DMI, Copenhagen, Available via http://megapoli.dmi.dk/publ/MEGAPOLI_sr10-04.pdf
24. Martilli A, Santiago J (2007) CFD simulation of airflow over a regular array of cubes. Part II: analysis of spatial average properties. Bound-Layer Meteorol 122(3):635–654
25. Ren Z, Wang X, Chen D, Wang C, Thatcher M (2014) Constructing weather data for building simulation considering urban heat island. Build Serv Eng Res Technol 35(1):69–82
26. Bueno B, Norford L, Hidalgo J, Pigeon G (2012) The urban weather generator. J Build Perform Simul 6(4):269–281
27. Massachusetts Institute of Technology (2015) Urban heat island effect modelling software: Urban Weather Generator version 3.0.0 MIT, Available via http://urbanmicroclimate.scripts.mit.edu/uwg.php. Accessed 26 Feb 2016
28. Arnfield AJ (2003) Two decades of urban climate research: a review of turbulence, exchanges of energy and water, and the urban heat island. Int J Climatol 23(1):1–26
29. Bouyer J, Inard C, Musy M (2011) Microclimatic coupling as a solution to improve building energy simulation in an urban context. Energy Buildings 43(7):1549–1559
30. Bourikas L et al (2013) Addressing the challenge of interpreting microclimatic weather data from urban sites. J Power Energy Eng 1:7–15
31. Shen T et al (2014) Impact of Urban Heat Island on Building Cooling Energy Consumption in Hangzhou. Abstracts of the 13th International Conference on Sustainable Energy Technologies, Geneva, Switzerland
32. Maxim Integrated (2013) iButton Temperature/Humidity logger with 8 kb data logger memory, Available via www.maximintegrated.com/products/ibutton/data-logging/
33. Shen T et al. (2013) Generating a modified weather data file for urban building design and sustainable urban planning accounting for the Urban Heat Island (UHI) effect. In: Abstracts of the 12th International Conference on Sustainable Energy Technologies, Hong Kong Polytechnic University, 26-29 August 2013.
34. Oke TR (2006) Initial guidance to obtain representative meteorological observations at urban sites. In: Instruments and observing methods Report No81, World Meteorological Organization. Available via www.wmo.int/pages/prog/www/IMOP/publications/IOM-81/IOM-81-UrbanMetObs.pdf. Accessed 26 Jan 2016.
35. Cheng H, Castro IP (2002) Near wall flow over urban-like roughness. Bound-Layer Meteorol 104(2):229–259
36. Stewart ID, Oke TR (2012) Local Climate Zones for Urban Temperature Studies. Bull Am Meteorol Soc 93(12):1879–1900
37. Google Earth (2013) Satellite Images of Hangzhou and Ningbo
38. Trimble Navigation Limited (2013) SketchUp 3D CAD software, Available via www.sketchup.com/
39. Xie Z, Castro IP (2006) Large-eddy simulation for urban micro-meteorology. J Hydrodynamics, Ser B 18(3, Supplement):259–264
40. Santiago J, Martilli A, Martín F (2007) CFD simulation of airflow over a regular array of cubes. Part I: Three-dimensional simulation of the flow and validation with wind-tunnel measurements. Bound-Layer Meteorol 122(3):609–634
41. Kanda M, Moriizumi T (2009) Momentum and Heat Transfer over Urban-like Surfaces. Bound-Layer Meteorol 131(3):385–401
42. Millward-Hopkins JT et al (2013) Aerodynamic Parameters of a UK City Derived from Morphological Data. Bound-Layer Meteorol 146(3):447–468
43. Bruse M, Fleer H (1998) Simulating surface–plant–air interactions inside urban environments with a three dimensional numerical model. Environ Model Softw 13(3–4):373–384
44. Wang H et al (2014) Feasibility and optimization of aerogel glazing system for building energy efficiency in different climates. Int J Low-Carbon Technol 0:1–8
45. Wang X, Altan H, Kang J (2015) Parametric study on the performance of green residential buildings in China. Frontiers of Archit Res 4(1):56–67
46. Middel A et al (2014) Impact of urban form and design on mid-afternoon microclimate in Phoenix Local Climate Zones. Landsc Urban Plan 122:16–28
47. Maggiotto G, Buccolieri R, Santo MA, Leo LS, Di Sabatino S (2014) Validation of temperature-perturbation and CFD-based modelling for the prediction of the thermal urban environment: the Lecce (IT) case study. Environ Model Softw 60:69–83
48. Nikolou S (2011) Low carbon city living in Guangzhou, China. Unpublished, MSc Thesis. University of Southampton, Southampton, UK
49. Yang X et al (2013) Evaluation of a microclimate model for predicting the thermal behavior of different ground surfaces. Build Environ 60:93–104
50. Willmott CJ (1982) Some comments on the evaluation of model performance. Bull Am Meteorol Soc 63(11):1309–1313
51. Hu T, Yoshino H, Jiang Z (2013) Analysis on urban residential energy consumption of Hot Summer & Cold Winter Zone in China. Sustainable Cities Society 6:85–91
52. National Centers for Environmental Prediction/National Weather Service/NOAA/U.S. Department of Commerce. 2000, updated daily. NCEP FNL Operational Model Global Tropospheric Analyses, continuing from July 1999. Research Data Archive at the National Center for Atmospheric Research, Computational and Information Systems Laboratory. dx.doi.org/10.5065/D6M043C6. Accessed 26 Jan 2016.
53. The Weather Underground (2014) Hangzhou weather data from Mantou mountain's National Principle WMO-listed weather station. www.wunderground.com. Accessed 26 Jan 2016